Investigation of Organoiron Catalysis in Kumada–Tamao–Corriu-Type Cross-Coupling Reaction Assisted by Solution-Phase X-ray Absorption Spectroscopy

AUTHOR(S):

Takaya, Hikaru; Nakajima, Sho; Nakagawa, Naohisa; Isozaki, Katsuhiro; Iwamoto, Takahiro; Imayoshi, Ryuji; Gower, Nicholas J.; ... Hashizume, Daisuke; Takahashi, Osamu; Nakamura, Masaharu

CITATION:

Takaya, Hikaru ...[et al]. Investigation of Organoiron Catalysis in Kumada–Tamao–Corriu-Type Cross-Coupling Reaction Assisted by Solution-Phase X-ray Absorption Spectroscopy. Bulletin of the Chemical Society of Japan 2015, 88(3): 410-418

ISSUE DATE:

2015

URL:

http://hdl.handle.net/2433/196165

Bull. Chem. Soc. Jpn. in press (doi:10.1246/bcsj.20140376)

Graphical Abstract

Investigation of Organoiron Catalysis in Kumada–Tamao–Corriu-Type Cross-Coupling Reaction Assisted by Solution-Phase X-ray Absorption Spectroscopy

H. Takaya, S. Nakajima, N. Nakagawa, K. Isozaki, T. Iwamoto, R. Imayoshi, N. J. Gower, L. Adak, T. Hatakeyama, T. Honma, M. Takagaki, Y. Sunada, H. Nagashima, D. Hashizume, O. Takahashi, and M. Nakamura

Solution-phase molecular structures of organoiron intermediates of Kumada–Tamao–Corriu-type cross-coupling were illuminated by X-ray absorption spectroscopy. The intermediacy of halomesityl iron complex of $Fe^{II}BrMes$(SciOPP) and dimesityl iron complex of $Fe^{II}Mes_2$(SciOPP) was adequately elucidated with formal non-redox Fe^{II}/Fe^{II} catalytic cycle.

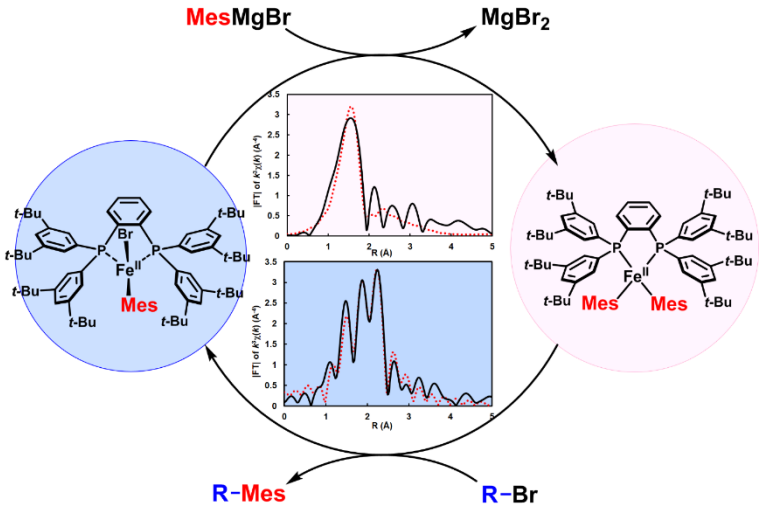

Investigation of Organoiron Catalysis in Kumada–Tamao–Corriu-Type Cross-Coupling Reaction Assisted by Solution-Phase X-ray Absorption Spectroscopy

Hikaru Takaya,*[a,b] Sho Nakajima,[a,b] Naohisa Nakagawa,[a] Katsuhiro Isozaki,[a,b,g] Takahiro Iwamoto,[a,b,g] Ryuji Imayoshi,[a,b] Nicholas J. Gower,[a] Laksmikanta Adak,[a] Takuji Hatakeyama,[a,b,h] Tetsuo Honma,[c] Masafumi Takagaki,[c] Yusuke Sunada,[d] Hideo Nagashima,[d,g] Daisuke Hashizume,[e] Osamu Takahashi,[f] and Masaharu Nakamura*[a,b]

[a]*International Research Center for Elements Science, Institute for Chemical Research, Kyoto University, Uji, Kyoto 611-0011, Japan. E-mail. takaya@scl.kyoto-u.ac.jp, masaharu@scl.kyoto-u.ac.jp*
[b]*Department of Energy and Hydrocarbon Chemistry, Graduate School of Engineering, Kyoto University, Kyoto 615-8510, Japan*
[c]*Japan Synchrotron Radiation Research Institute (JASRI, SPring-8), Sayo, Hyogo 679-5198, Japan*
[d]*Division of Applied Molecular Chemistry, Institute for Materials Chemistry and Engineering, Kyushu University, Fukuoka 816-8580, Japan*
[e]*Center for Emergent Matter Science, RIKEN, Wako, Saitama 351-0198, Japan*
[f]*Institute for Sustainable Sciences and Development, Hiroshima University, Higashi-Hiroshima 739-8511, Japan*
[g]*CREST, Japan Science and Technology Agency (JST)*
[h]*Element Strategy Initiative for Catalyst and Battery, Kyoto University, Kyoto 615-8510, Japan*

Received: November 29, 2014; E-mail: takaya@scl.kyoto-u.ac.jp

Synopsis

Solution-phase synchrotron X-ray absorption spectroscopy (XAS) is a powerful tool for structural and mechanistic investigations of paramagnetic organoiron intermediates in solution-phase reactions. For paramagnetic organotransition metal intermediates, difficulties are often encountered with conventional NMR- and EPR-based analyses. By using solution-phase XAS, we succeeded in identifying the organoiron species formed in the reaction of iron bisphosphine with mesitylmagnesium bromide, MesMgBr, and 1-bromodecane in a FeX_2(SciOPP)-catalyzed Kumada–Tamao–Corriu (KTC)-type cross-coupling reaction. X-ray absorption near-edge structure (XANES) spectra showed that the resulting aryliron species possessed a divalent oxidation state. Extended X-ray absorption fine structure (EXAFS) demonstrated that the solution-phase molecular geometries of these species are in satisfactory agreement with the crystallographic geometries of Fe^{II}BrMes(SciOPP) and $Fe^{II}Mes_2$(SciOPP). By combining GC-quantitative analysis and solution-phase XAS, the cross-coupling reactivities of these aryliron

species were successfully investigated in the reaction with 1-bromodecane under stoichiometric and catalytic conditions.

Introduction

The renaissance of iron-catalyzed cross-coupling reactions in the last decade[1–5] has been triggered by their unprecedented non-classical reactivities and selectivities in comparison with conventional Pd and Ni catalysts.[6] Recent worldwide interest in practical research applications, based on the utilization of abundant earth elementsand the practical advantages of iron catalysts, including low cost, low toxicity, high availability, easy separation of metal residues, have also demanded a much greater focus on iron-catalyzed cross-coupling reactions. These reactions had been overlooked for over 30 years[7–10] since they were first discovered by Kochi.[11] Recently, there has been significant progress in cross-coupling technology based on several 3d transition metal catalysts, such as Cr,[12] Mn,[13] Co,[14] Ni,[15] Cu,[16,17] and as well as Fe catalysts.[18–26] Despite this, large paramagnetic shifts and related loss of spin–spin coupling information in the NMR spectra hamper the solution-phase structural studies of catalytic intermediates in the reaction mixture.[27] Conventional EPR spectroscopy also suffers from difficulties with typical Fe^{II} and Fe^{III} species having S = 1 and 2, which are often invisible to this technique. In addition, traditional mechanistic studies based on X-ray crystallography of isolated intermediates are often difficult to perform because of the instability of the 3d metal–carbon bonds when exposed to air and moisture. We therefore envisioned applying synchrotron X-ray absorption spectroscopy (XAS) to the structural and mechanistic investigation of paramagnetic organometallic intermediates in homogeneous iron-catalyzed reactions. XAS analysis enables the determination of the charge state and the precise local geometry of the observed element without being affected by the paramagnetic property of the target element. Despite the widespread application and significant contribution of synchrotron XAS in the investigation of heterogeneous catalysts,[28] its use with homogeneous catalysts[29] remains underdeveloped,

though intensive research is ongoing.[30–32] To the best of our knowledge, Stults and co-workers were the first to demonstrate the effectiveness of XAS to investigate non-aqueous, homogeneous catalytic systems. This was accomplished through the structure determination of catalytic intermediates of rhodium bisphosphine-catalyzed asymmetric hydrogenation, which was successfully achieved through the combined use of solution-phase XAS, NMR, and X-ray crystallography.[33] More recently, Evans and co-workers have taken the lead in the practical applications of solution-phase XAS through comprehensive XAS-based studies conducted on homogeneous organonickel species.[34] Recent progress in X-ray spectroscopy, based on the ultra-high brilliant third-generation synchrotron X-ray, made solution-phase XAS widely accessible for the *in situ* structural investigation of various organometallic species.[35,36] Remarkable results have been achieved in the structural investigation of paramagnetic 3d transition-metal-based catalysts such as Cr,[37] Mn,[38] Co,[39] Ni,[40] and Cu.[41] However, there has been minimal research on solution-phase XAS studies of organoiron species. This is because the larger multiplicity of high spin d^6 Fe^{II}- and d^5 Fe^{III}-XAS,[42] compared with other 3d transition metals, hampers the interpretation and assignment of the spectra, along with peak broadening arising from the fluxional behavior of molecules in the solution. Recently, pioneering research on homogeneous iron catalysis has been conducted by Bauer and co-workers,[43,44] including Fe-catalyzed KTC-type cross-coupling reactions.[45] Formation of monovalent iron species by the reaction of $Fe(acac)_3$ with over three molar equivalents of PhMgCl in THF/NMP was confirmed. This proved to be a catalytically active species for the cross-coupling of aryl chlorides and primary alkyl Grignard reagents.[7,8,10] In addition, Neidig recently demonstrated that the combined use of magnetic circular dichroism and Mössbauer spectroscopy provides an efficient solution for the mechanistic investigation of homogeneous organoiron catalysts derived from FeX_2(SciOPP).[46] As discussed later, this approach has advantages for analysis of mixtures that contain multiple intermediates because of the better peak resolution of Mössbauer spectroscopy compared with XAS.

Herein, we report the solution-phase XAS-assisted identification and structural determination of the organoiron intermediates that are present in Fe-catalyzed KTC-type cross-coupling reactions. The fingerprint analysis of XANES and spectrum fitting analysis of EXAFS in the K-edge region were successfully demonstrated as efficient methods for the solution-phase structural study of paramagnetic organoiron intermediates. The KTC-type cross-coupling reaction is commonly categorized as Ni- or Pd-catalyzed cross-coupling of alkyl halides/aryl halides with Grignard reagents. The broad scope of substrates makes this reaction a powerful tool for carbon–carbon bond framework construction in synthetic organic chemistry. Ni^{0}/Ni^{II} and Pd^{0}/Pd^{II} redox mechanisms are widely investigated[6,15] as they can be easily studied by solution-phase NMR spectroscopy. On the other hand, mechanistic research on Fe-catalyzed KTC-type reactions still provokes much debate, despite this type of reaction being the most widely studied among the Fe-catalyzed cross-coupling reactions.[1–5] Various mechanisms have been proposed with Fe^{I}/Fe^{III}, Fe^{0}/Fe^{II}, and Fe^{-II}/Fe^{0} catalytic cycles, which were inferred from product distributions of reactions using various stoichiometries of Grignard reagents, the stereochemistry, kinetic experiments, and reactivities toward radical-probing substrates. Recently, we have developed an iron bisphosphine complex, $Fe^{II}X_2$(SciOPP),[24] which has proven to be particularly effective towards KTC-type cross-coupling reactions.[47,48] Here, the abbreviation SciOPP (spin-control-intended *o*-phenylene bisphosphine) for the bisphosphine ligand 1,2-bis[bis{3,5-di(*t*-butyl)phenyl}phosphino]benzene originates from the concept of the spin-state control of a catalytic metal center. For the $Fe^{II}X_2$(SciOPP)-catalyzed KTC-type cross-coupling, we proposed a formal non-redox Fe^{II}/Fe^{II} mechanism involving transmetalation of the (halo)aryl intermediate Fe^{II}XAr(SciOPP) with aryl Grignard reagents ArMgX and cross-coupling of the diaryl iron intermediate $Fe^{II}Ar_2$(SciOPP) with an alkyl halide (R–X), as shown in Scheme 1. This mechanism was inferred from previous studies on the FeX_n-tmeda system,[9,49] in which isolation and the crystal structure determination of organoiron complexes Fe^{II}BrMes(tmeda) and $Fe^{II}Mes_2$(tmeda) were successfully achieved to demonstrate their

intermediacy in the KTC-type cross-coupling reaction. The reactions with radical-probing substrates support that $Fe^{II}Mes_2(tmeda)$ predominantly reacts with alkyl halides through the

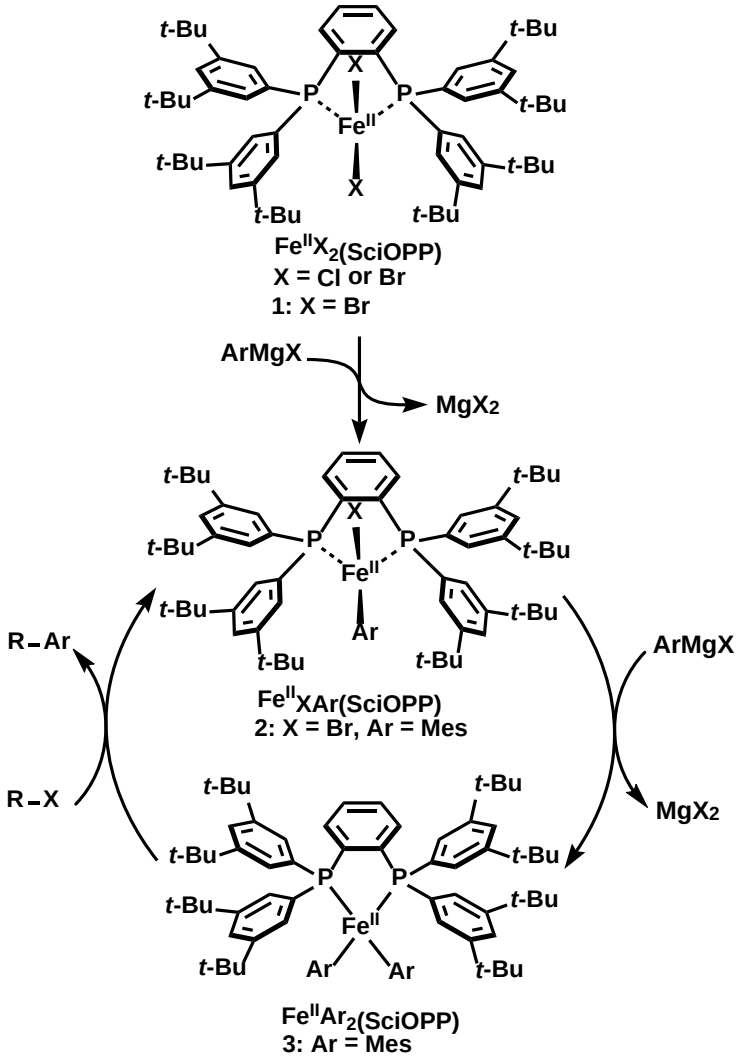

Scheme 1. Proposed mechanism for $Fe^{II}X_2$(SciOPP)-catalyzed KTC-type cross-coupling of an arylmagnesium halide with an alkylhalide.

homolytic cleavage of a carbon–halogen bond, followed by coupling of the resultant alkyl radical and mesityl radical, derived from $Fe^{II}Mes_2(tmeda)$, to yield the cross-coupling product (R–Ar). Recently, Bedford[50] reported that trimesityl ferrate species[51] $[Fe^{II}Mes_3]^-$ were the primary responsible catalytic species in the $FeCl_2$-tmeda-catalyzed cross-coupling reaction of MesMgX with primary alkyl halides. However, Fürstner[52] individually indicated the higher responsibility of $FeMes_2(L)$ (L = tmeda and SciOPP) for this reaction rather than $[Fe^{II}Mes_3]^-$

with negligibly small amounts of Mes-Mes byproduct. These findings have further complicated determination of the mechanism of the Fe-catalyzed KTC-type reaction. We propose that direct *in situ* observation of organoiron intermediates by means of solution-phase XAS can settle such debates generated by indirect approaches using product analysis and kinetic experiments, even with crystallographically characterized intermediates. To elucidate ambiguities in the reaction mechanism, we conducted a solution-phase XAS study where the objective was to confirm the solution-state valence and structures of the organoiron intermediates engaged in the abovementioned mechanism for the $Fe^{II}X_2$(SciOPP)-catalyzed KTC-type reaction.

Results and discussion

Synthesis and crystallographic characterization

To obtain pure samples of the proposed (halo)aryliron and diaryliron intermediates, we prepared analytically pure organoiron species of Fe^{II}BrMes(SciOPP) **2** and $Fe^{II}Mes_2$(SciOPP) **3**. As described later, the crystallographic coordinates obtained from these complexes were used for the theoretical calculation of the XANES spectrum and EXAFS fitting analyses. Equations (1) and (2) show multigram-scale synthetic procedures for the preparation of organoiron species

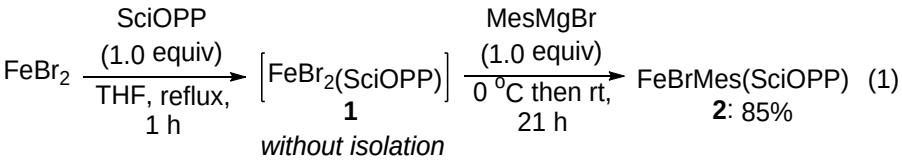

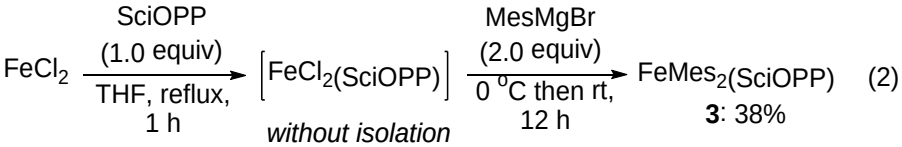

2 and **3** under the corresponding KTC-type cross-coupling conditions. The reaction of *in situ* generated $Fe^{II}Br_2$(SciOPP) **1** with 1.0 equivalent of MesMgBr yielded (halo)aryliron complex **2** as a yellow powder. Similarly, the addition of 2.0 equivalents of MesMgBr to *in situ* generated

$Fe^{II}Cl_2$(SciOPP) yielded the corresponding diaryliron complex **3** as a dark-red powder.[53] The ^{1}H NMR spectra of mesityl iron complexes **2** and **3** exhibited large paramagnetic shifts and the broadening of signals (see SI Figures S33–S36). The solution-phase effective magnetic moment (μ_{eff} = 4.9) for **2**, measured by the Evans' method in THF-d_8, is consistent with the spin-only value of 4.9, which is expected for high-spin (S = 2) tetrahedral (bromo)mesityliron bisphosphine complexes with four unpaired electrons (see SI Figure S3). In contrast, the magnetic moment of dimesityl complex **3** produced a μ_{eff} value of 4.1, which is significantly different from the spin-only value of 2.8 for S = 1 square-planar iron complexes with two unpaired electrons (see SI Figure S4). However, a similar inconsistency in the μ_{eff} values of square-planar diaryliron complexes has been previously reported for *cis*-$Fe^{II}Mes_2$(dppe) (μ_{eff} = 3.3–3.9)[54,55] and *trans*-$Fe^{II}(C_6Cl_5)_2(PEt_2Ph)_2$ (μ_{eff} = 3.6).[54] Note that such large deviations from the spin-only μ_{eff} values of square planar divalent iron complexes have also been reported for divalent iron porphyrin[56] and phthalocyanine[57] complexes (μ_{eff} = 4.0–4.9), and that these phenomena were consistently explained by their anomalous electronic configurations with extremely large g-values.

Single crystal X-ray crystallographic determination of mesityliron complexes **2** and **3** were successfully performed using synchrotron radiation at the BL40XU and BL02B1 beamlines of SPring-8 (Figures 1a and 1b). The X-ray structural determination of **3** was unprecedented for a square-planar diaryliron(II) bisphosphine complex. The observed Fe–P bond lengths in **2** (2.4575(8) and 2.4430(7) Å) are similar to those of the analogous complex Fe^{II}ClMes(dppe) (2.5169(15) and 2.4598(15) Å)[54] and those of the starting $Fe^{II}Br_2$(SciOPP) **1** (2.4610(11) and 2.4249(11) Å) and are within a reasonable range for high-spin tetrahedral divalent iron bisphosphine complexes.[24,54,58] The relatively short Fe–P bond length of **3** (2.2949(8) Å) is consistent with the bond lengths previously reported for intermediate-spin (S = 1) iron complexes.[54]

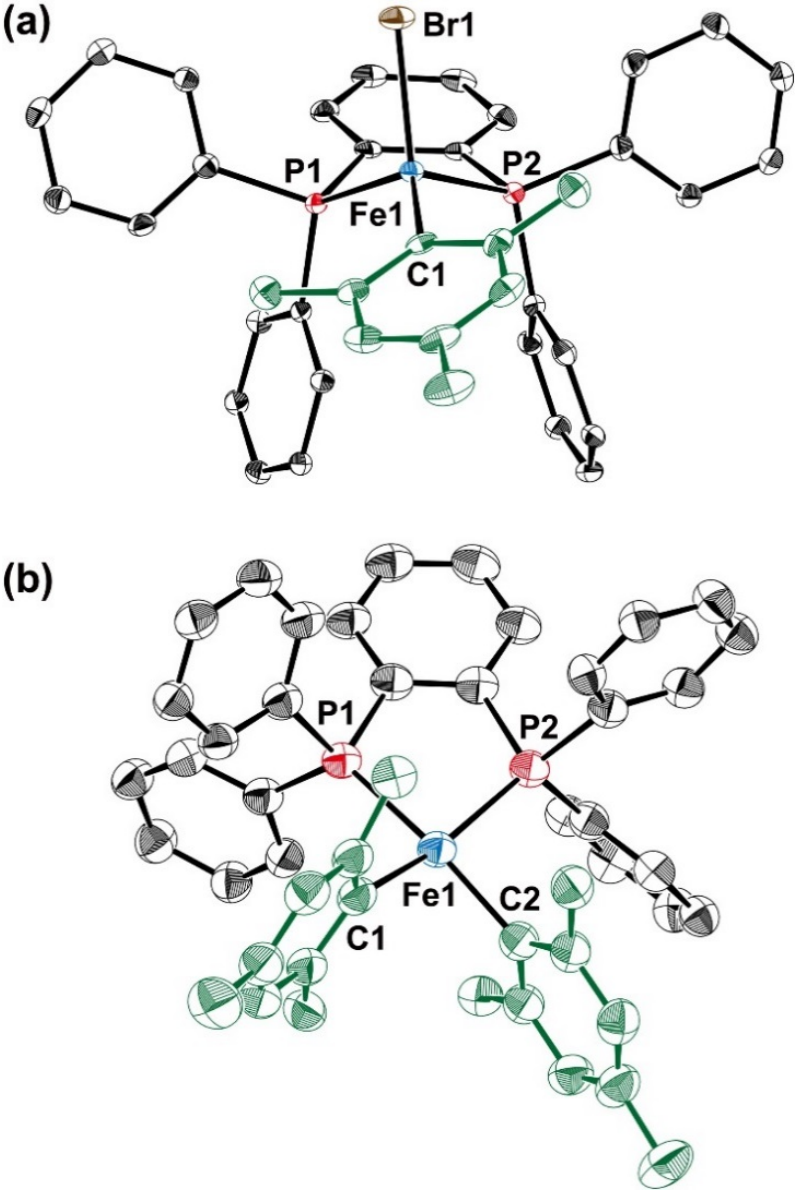

Figure 1. Molecular structure determined by single crystal X-ray crystallography for (a) $Fe^{II}BrMes(SciOPP)$ **2**, and (b) $Fe^{II}Mes_2(SciOPP)$ **3**. Ellipsoids are at the 50% probability level. Carbon-bound hydrogen atoms and *t*-Bu groups are omitted for clarity. Selected bond lengths and angles for **2**: Fe1–Br1 2.4182(5) Å, Fe1–P1 2.4575(8) Å, Fe1–P2 2.4430(7) Å, Fe–C1 2.046(3) Å, P1–Fe1–C1 124.86(8)°, P2–Fe1–C1 119.72(8)°, P1–Fe1–Br1 96.97(2)°, P2–Fe1–Br1 100.19(2)°, P1–Fe1–P2 78.33(2)°, C1–Fe1–Br1 125.38(8)°. Selected bond lengths and angles for **3**: Fe1–P1 2.2874(7) Å, Fe1–P2 2.2874(7) Å, Fe1–C1 2.020(2) Å, Fe1–C2 2.020(2) Å, P1–Fe1–C1 93.43(7)°, P2–Fe1–C2 93.43(7)°, P1–Fe1–P2 83.99(2)°, C1–Fe1–C2 92.7(1)°.

Solution-phase XAS study

The applicability of the solution-phase XAS analysis was examined by comparing the crystalline solid-phase and THF solution-phase spectra of isolated **2** and **3** through the use of synchrotron radiation at SPring-8, BL14B2 beamline.[59] As shown in Figure 2a, the corresponding Fe K-edge XANES spectra of the powder sample diluted with boron nitride and the solution sample of (bromo)mesityliron **2** in THF are very similar, indicating that the valence and geometry observed in the crystalline solid-phase remains unchanged in solution-phase. The decent resemblance between the pre-edge region and the peak at 7109.5 eV, ascribed to the 1s–3d electron transition with 3d–4p orbital mixing in tetrahedral iron(II) complexes,[42,60,61] also demonstrates the preservation of solid-phase molecular geometry in solution-phase. The geometrical similarity of dimesityliron **3** in the crystalline- and THF solution-phases was also demonstrated by the excellent agreement of the corresponding XANES spectra (Figure 2b). The shoulder-edge peak at around 7115.2 eV was assumed to be a 1s–4p_z transition that was induced by the square-planar geometry of the 3d transition metal complexes.[60,61] This indicates that the square-planar geometry of **3**, confirmed by X-ray crystallography, was preserved in the THF solution. The assignment is still speculative because there is almost no information on the XANES analysis of diaryliron complexes, despite the isolation of several four-coordinate, square planar dimesityliron(II) phosphine complexes, such as *cis*-$Fe^{II}Mes_2(dppe)$[54,55] and *trans*-$Fe^{II}Mes_2(PR_3)_2$ complexes.[54] Spectrum simulation by a DFT-level core excitation calculation gave a reasonable result for the 1s-4p_z edge peak of the XANES spectrum of square-planar **3** (see SI Figure S24). Adequate matching of EXAFS regions of crystalline- and solution-phase **2** and **3** was also confirmed in real *k*-spaces (see SI Figures S6 and S8).

The solution-phase structure determination of **2** and **3** was conducted using the obtained EXAFS spectra and crystallographic atomic coordinates. As shown in Figures 3a and 3b, EXAFS data analysis[62] was conducted using fitting simulation based on multiple-scattering

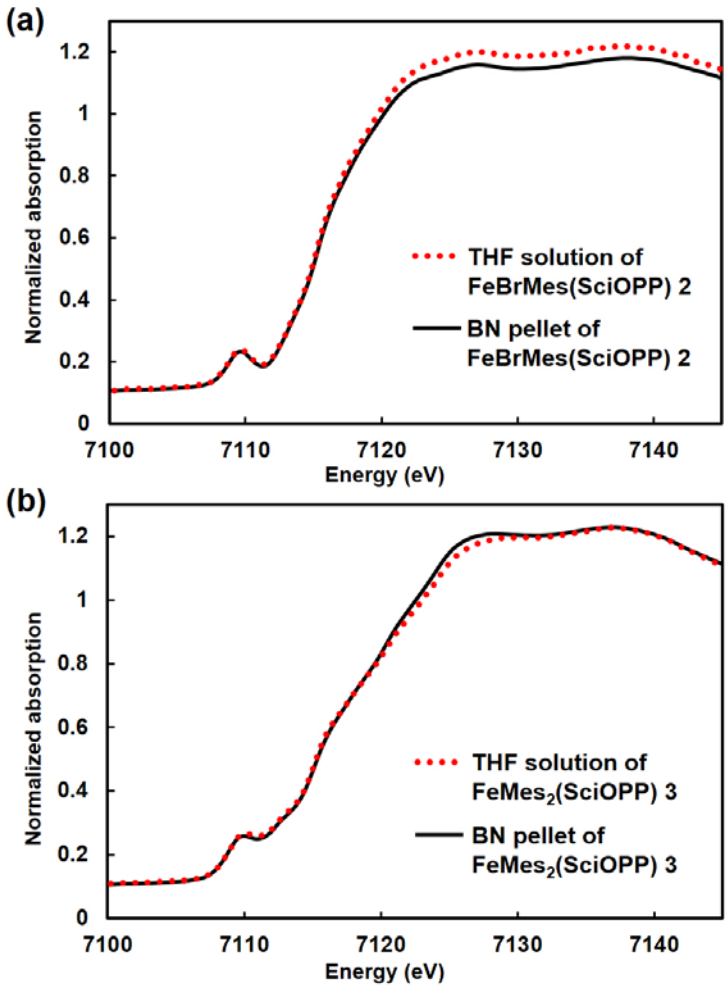

Figure 2. The solution-phase Fe K-edge XANES spectra for organoiron intermediates **2** and **3** superimposed on the corresponding solid-phase spectra. (a) XANES spectra of THF solution (red dotted line) and BN diluted pellet of **2** (black line). (b) XANES spectra of THF solution (red dotted line) and BN diluted pellet of **3** (black line).

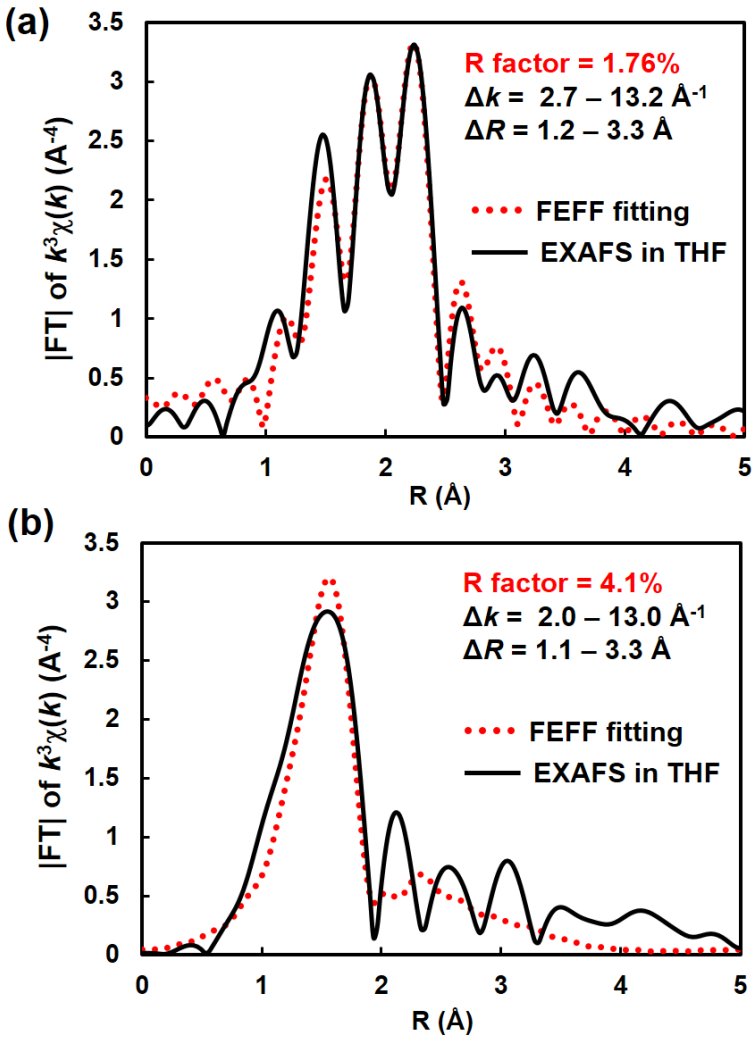

Figure 3. Solution-phase EXAFS fitting analysis for organoiron intermediates **2** and **3**. (a) Solution-phase EXAFS spectrum of **2** (black line) without phase shift correction and the FEFF-calculated fit (red dotted line). (b) Solution-phase EXAFS spectrum of **3** (black line) without phase shift correction and the FEFF-calculated fit (red dotted line).

paths calculation. This demonstrated that the molecular structures of **2** and **3** in THF are similar to the crystallographic structures, maintaining their original local geometries around the Fe centers in terms of the lengths and angles of the Fe–Br, Fe–P, and Fe–C bonds. The observed deviation of the solution-phase geometries from the crystallographic geometries in the small radius region around R = 1.0–1.7 Å is caused by coordination of THF molecules, as reported by Tanaka[40] and Bauer.[45] The relatively larger error observed in **3** with a higher R factor of 4.7% can be ascribed to the better solvent accessibility of the unoccupied d_z^2 axis of its square-planar

structure. The EXAFS analysis performed for the catalyst precursor $Fe^{II}Br_2$(SciOPP) **1** also confirmed that there were almost no structural differences between the solution-phase and crystalline-phase (see SI Figures S9–S11). These results show that the identification and structural determination of the organoiron intermediates by solution-phase XAS analysis are adequately feasible.

Solution-phase *in situ* XAS study of KTC coupling

To assess the formation of the proposed organoiron intermediates **2** and **3** in the $Fe^{II}X_2$(SciOPP)-catalyzed KTC-type cross-coupling reaction, *in situ* XAS monitoring of the stoichiometric reaction of $Fe^{II}Br_2$(SciOPP) **1** with Grignard reagent MesMgBr in THF was conducted at ratios of 1:1 and 1:2. It was found that the use of the iron dibromide complex $Fe^{II}Br_2$(SciOPP) **1** rather than the dichloride complex $Fe^{II}Cl_2$(SciOPP) enabled us to avoid chlorine–bromine exchange with MesMgBr and to obtain a Br K-edge XAS observation of the transmetalation pathway. Figure 4a shows the Fe K-edge XANES spectra of a solution of **1** in THF and reaction mixtures obtained by adding 1.0 or 2.0 equivalents of MesMgBr to **1**. For the solution to which 1.0 equivalent of MesMgBr was added, compared with **1**, a negligibly small energy shift of the rising edge and an increase in pre-edge peak height at 7109.5 eV were observed. This indicates that the iron center remains divalent, and the formation of monomesityl iron Fe^{II}BrMes(SciOPP) **2** was identified by comparison with the XANES and EXAFS spectra of pure **2** in THF (see SI Figures S12 and S13). The lowered centrosymmetry of **2** compared with **1**, upon the substitution of one Br ligand with Mes, increases the amount of 3d–4p orbital mixing along with the intense pre-edge peak. With the addition of 2.0 equivalents of MesMgBr, the formation of the divalent dimesityliron species $Fe^{II}Mes_2$(SciOPP) **3** was identified,[63] with the appearance of a $1s–4p_z$ transition around 7112.3 eV which was induced by the geometry change from tetrahedral to square-planar, as described above. Figure 4b shows the superimposed EXAFS spectra for **1**, as well as for **1** with 1.0 and 2.0 equivalents of MesMgBr. Drastic changes,

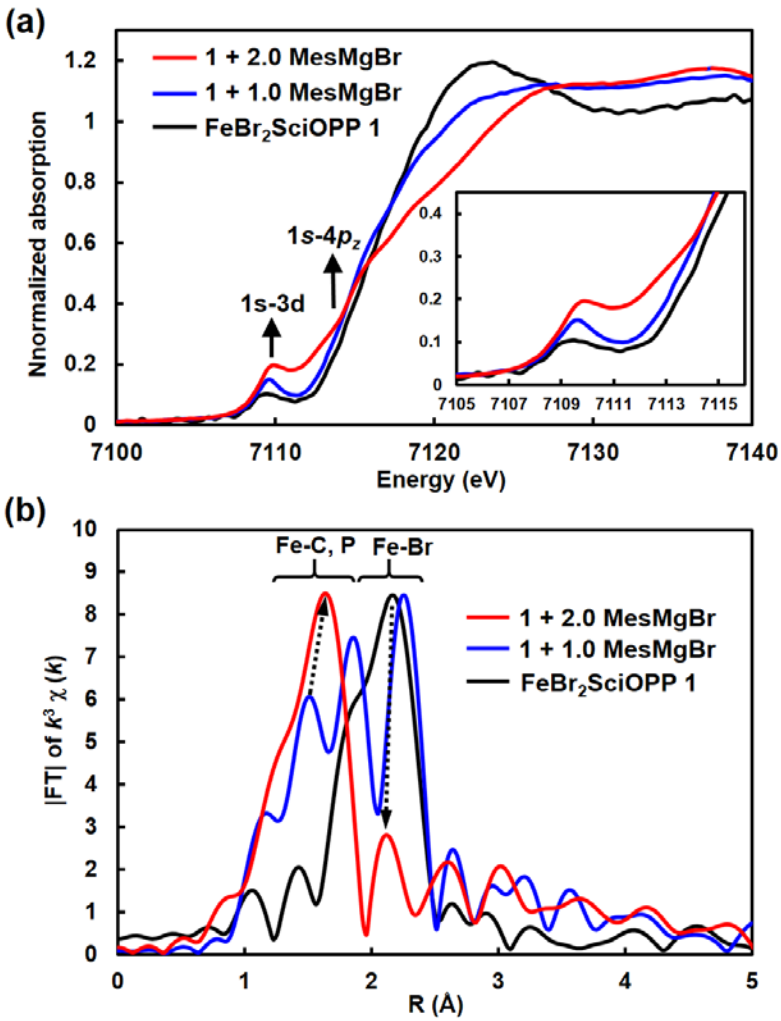

Figure 4. The XAS-based quantitative analysis of the formation of organoiron intermediates **2** and **3**. (a) A series of Fe K-edge XANES spectra for THF solutions of **1** (black line), reaction mixtures of **1** with 1.0 equivalent (blue line), and 2.0 equivalents (red line) of MesMgBr. (b) A series of Fe K-edge EXAFS spectra for THF solutions of **1** (black line), reaction mixtures of **1** with 1.0 equivalent (blue line), and 2.0 equivalents (red line) of MesMgBr without phase shift correction.

compared with the spectrum of **1**, were observed along with the loss of the peak at around 2.17 Å, accompanied by the appearance of new peaks at around 1.0–2.0 Å. These changes can be attributed to the conversion of Fe–Br bonds to Fe–C bonds, resulting from bromide exchange with the mesityl ligand, yielding the corresponding (bromo)mesityl and dimesityl complexes **2** and **3**. A decreasing peak for Fe–Br bond was also confirmed in the corresponding Br K-edge

EXAFS spectra (see SI Figure S16).

The cross-coupling activities of the isolated ironmesityl complexes **2** and **3** were assessed by stoichiometric reactions with 1-bromodecane (**4**, Decyl–Br). *In situ* XAS analysis (vide infra) of the reaction mixtures gave the results described in equation (3); the corresponding product yield was determined by GC analysis based on the amounts of starting iron complex. For this

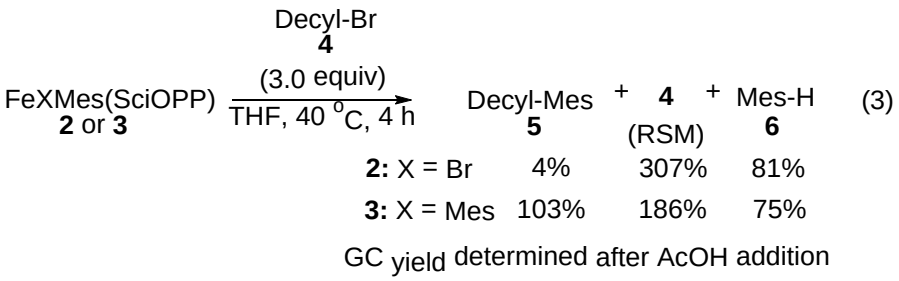

coupling reaction, dimesityliron **3** yielded the coupling product 1-decyl-2,4,6-trimethylbenzene (**5**, Decyl–Mes) in 103% yield (see SI Table S1 and Figure S1). On the other hand, monomesityliron **2** gave **5** in 4% yield.

These results clearly demonstrate the substantially higher cross-coupling reactivity of **3** compared with that of **2**. The observed contrasting reactivities of **2** and **3** were confirmed by XANES and EXAFS analyses of the reaction mixtures. In the reaction mixture of **3** with **4**, the formation of **2** from **3** was observed with less than 10% unreacted **3** (see SI Figures S20 and S21). On the other hand, in the reaction mixture of **2** with **4**, unreacted **2** was predominantly detected (see SI Figures S17–S19). These results suggest that $Fe^{II}Mes_2$(SciOPP) **3** acts as an active catalytic species and Fe^{II}BrMes(SciOPP) **2** is a substantially less reactive resting species for the Decyl–Mes coupling step, as depicted in the mechanism shown in Scheme 1. The mass balance of recovered starting bromoalkane **4** and mesitylene (**6**, Mes–H) was determined by GC-analysis after the acid quenching of the unreacted iron mesityl species. The results indicated that one of two mesityl ligands of **3** can react with an alkyl halide to yield monomesityliron intermediate **2**, corresponding well with the **2**- and **3**-based Fe^{II}/Fe^{II} catalytic cycle.

Finally, we examined the catalytic activity of **3**. This was done through the reaction of **4** with PhMgBr, in the presence of 10 mol% of **3**. As shown in equation (4), the catalytic activity of **3** was determined to yield 16% of **5** and 50% of 1-decylbenzene (Decyl–Ph), along with 10% debrominated by-products and 15% of the starting bromoalkane **4**.

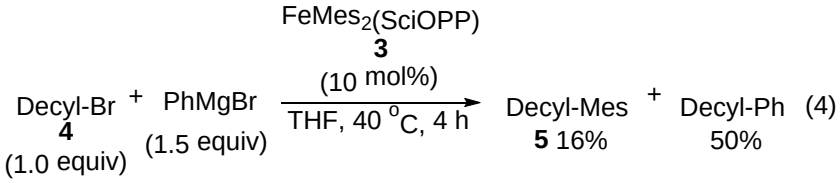

Conclusions

We have successfully synthesized two paramagnetic organoiron complexes, (bromo)mesityl-iron(II) complex $Fe^{II}BrMes(SciOPP)$ **2** and dimesityliron(II) complex $Fe^{II}Mes_2(SciOPP)$ **3**, by the reaction of MesMgBr and $Fe^{II}X_2(SciOPP)$. The molecular structures of **2** and **3** were unequivocally determined by single crystal X-ray crystallography with tetrahedral and square-planar geometries, respectively. The solution-phase molecular structures of **2** and **3** were also elucidated via EXAFS fitting analysis with use of atomic coordinates obtained by X-ray crystallography. The efficiency of the solution-phase *in situ* XAS analysis was demonstrated by direct observation of the formation of **2** and **3** from **1** with MesMgBr and cross-coupling reactivities of **2** and **3** with 1-bromodecane **4**. The XAS-based mechanistic investigations of paramagnetic iron catalysis, which is difficult by conventional NMR, corroborated the proposed Fe^{II}/Fe^{II} mechanism for the $Fe^{II}X_2(SciOPP)$-catalyzed KTC-type cross-coupling reaction. As mentioned above, because of the lower peak resolution of EXAFS compared with Mössbauer spectroscopy, there still appears to be redundancy in the mixture system. However, a statistical approach based on factor analysis can solve this issue to provide peak separation of independent species, enabling the structure determination of each species, as Tanaka and co-workers demostrated.[40] The significant advantage of solution-phase XAS encouraged us to extend the

research target to other paramagnetic 3d transition-metal-catalyzed reactions in which air- and moisture-sensitive paramagnetic organo-Cr, -Mn, -Co, -Ni, and -Cu species act as the catalytic intermediate.

Acknowledgements

This work was supported by “Funding Program for Next generation World-Leading Researchers (Next Program)” initiated by the Council for Science & Technology Policy (CSTP), CREST (1102545 & 11103784) programs from Japan Science & Technology Agency (JST), a Grant-in-Aid for Scientific Research (22550099) from the Ministry of Education, Culture, Sports, Science & Technology (MEXT), and through the JSPS. The synchrotron XAFS and single-crystal X-ray analysis were performed at SPring-8 beam lines of BL14B2, BL27Su, BL02B1, and BL40XU with the approval of JASRI (BL14B2: 2014A1565, 2013B1855, 2013B1717, 2013A1601, 2013A1798, 2012B1737, 2012A1595, 2011B1945, and 2009B1462; BL27Su: 2014A1740, 2013B1115, 2013A1685, and 2012B1797; BL02B1 2013A1661 and 2013B1126; BL40XU: 2014A1717, 2013B1736, 2013A1705, 2012B1815, 2012A1625, and 2011B1545). The authors express deep gratitude to Prof. Masayuki Nihei for his advice and discussion about anomalous magnetic susceptibility of square planar iron complexes. The authors thank Ms Toshiko Hirano (ICR Kyoto Univ.) for elemental analysis. The authors also thanks Dr. Kazuki Ogata for his preliminary experiments to synthesize $FeBr_2$SciOPP. S.N. expresses his deep gratitude to the Sumitomo Fellowship program. N.N. expresses his special thanks to the ICR exchange program going abroad. N.G. & L.A. express their special thanks for JSPS fellowship (24·02790 & 24·02338) for financial support.

Supporting Information

Synthesis and characterization of organoiron complexes, reaction procedure, XAS measurement, and X-ray data. This material is available electronically on J-STAGE.

Notes and references

1. A. Leitner, *Iron Catalysis in Organic Chemistry*, ed. By B. Plietker, Wiley-VCH, Weinheim, **2008**, pp. 147–176.
2. E. Nakamura, T. Hatakeyama, S. Ito, K. Ishizuka, L. Ilies, M. Nakamura, *Org. React.*, **2014**, *83*, 1.
3. L. Ilies, E. Nakamura, *PATAI's Chemistry of Functional Groups: The Chemistry of Organoiron Compounds*, ed. by I. Marek and Z. Rappoport, John Wiley & Sons, New York, **2014**, pp. 539–568.
4. B. D. Sherry, A. Fürstner, *Acc. Chem. Res.*, **2008**, *41*, 1500.
5. E. Nakamura, Y. Yoshikai, *J. Org. Chem.*, **2010**, *75*, 6061.
6. R. Jana, T. P. Pathak, M. S. Sigman, *Chem. Rev.*, **2011**, *111*, 1417.
7. G. Cahiez, S. Marquais, *Tetrahedron Lett.*, **1996**, *37*, 1773.
8. A. Fürstner, A. Leitner, M. Méndez, H. Krause, *J. Am. Chem. Soc.*, **2002**, *124*, 13856.
9. M. Nakamura, K. Matsuo, S. Ito, E. Nakamura, *J. Am. Chem. Soc.*, **2004**, *126*, 3686.
10. T. Nagano, T. Hayashi, *Org. Lett.*, **2004**, *6*, 1297.
11. M. Tamura, J. K. Kochi, *J. Am. Chem. Soc.*, **1971**, *93*, 1487.
12. A. K. Steib, O. M. Kuzmina, S. Fernandez, D. Flubacher, P. Knochel, *J. Am. Chem. Soc.*, **2013**, *135*, 15346.
13. G. Cahiez, A. Moyeux, *Chem. Rev.*, **2010**, *110*, 1435.
14. J. Terao, N. Kambe, *Acc. Chem. Res.*, **2008**, *41*, 1545.
15. I. P. Beletskaya, A. V. Cheprakov, *Organometallics*, **2012**, *31*, 7753.
16. J. Terao, H. Todo, S. A. Begum, H. Kuniyasu, N. Kambe, *Angew. Chem. Int. Ed.*, **2007**, *46*, 2086.
17. C.-T. Yang, Z.-Q. Zhang, J. Liang, J.-H. Liu, X.-Y. Lu, H.-H. Chen, L. Liu, *J. Am. Chem. Soc.*, **2012**, *134*, 11124.

18. G. Cahiez, O. Gager, F. Lecomte, *Org. Lett.*, **2008**, *10*, 5255.
19. G. Cahiez, V. Habiak, C. Duplais, A. Moyeux, *Angew. Chem. Int. Ed.*, **2007**, *46*, 4364.
20. T. Hatakeyama, M. Nakamura, *J. Am. Chem. Soc.*, **2007**, *129*, 9844.
21. G. Cahiez, L. Foulgoc, A. Moyeux, *Angew. Chem. Int. Ed.*, **2009**, *48*, 2969.
22. A. Fürstner, R. Martin, H. Krause, G. Seidel, R. Goddard, C. W. Lehmann, *J. Am. Chem. Soc.*, **2008**, *130*, 8773.
23. T. Hatakeyama, S. Hashimoto, K. Ishizuka, M. Nakamura, *J. Am. Chem. Soc.*, **2009**, *131*, 11949.
24. T. Hatakeyama, T. Hashimoto, Y. Kondo, Y. Fujiwara, H. Seike, H. Takaya, Y. Tamada, T. Ono, M. Nakamura, *J. Am. Chem. Soc.*, **2010**, *132*, 10674.
25. C. J. Adams, R. B. Bedford, E. Carter, N. J. Gower, M. F. Haddow, J. N. Harvey, M. Huwe, M. Á. Cartes, S. M. Mansell, C. Mendoza, D. M. Murphy, E. C. Neeve, J. Nunn, *J. Am. Chem. Soc.*, **2012**, *134*, 10333.
26. R. B. Bedford, E. Carter, P. M. Cogswell, N. J. Gower, M. F. Haddow, J. N. Harvey, D. M. Murphy, E. C. Neeve, J. Nunn, *Angew. Chem. Int. Ed.*, **2013**, *52*, 1285.
27. I. Bertini, C. Luchinat, and G. Parigi, *Solution NMR of Paramagnetic Molecules: Applications to Metallobiomolecules and Models, Current Methods in Inorganic Chemistry Vol 2*, Elsevier, Amsterdam, **2001**, pp 143–203.
28. S. Bordiga, E. Groppo, G. Agostini, J. A. van Bokhoven, C. Lamberti, *Chem. Rev.*, **2013**, *113*, 1736.
29. H. Bertagnolli, T. S. Ertel, *Angew. Chem. Int. Ed. Engl.*, **1994**, *33*, 45.
30. M. Bauer, G. Heusel, S. Mangold, H. Bertagnolli, *J. Synchrotron Rad.*, **2010**, *17*, 273.
31. R. C. Nelson, J. T. Miller, *Catal. Sci. Technol.*, **2012**, *2*, 461.
32. S. G. Fiddy, J. Evans, T. Neisius, M. A. Newton, N. Tsoureas, A. D. Arran, A. A. Danopouuos, *Chem. Eur. J.*, **2007**, *13*, 3652.
33. B. R. Stults, R. M. Friedman, K. Koenig, W. S. Knowles, R. B. Greegor, F. W. Lytle, *J. Am.*

Chem. Soc., **1981**, *103*, 3235.

34. (a) J. M. Corker, J. Evans, H. Leach, W. Levason, *J. Chem. Soc., Chem. Commun.*, **1989**, 181; (b) J. M. Croker and J. Evans, *J. Chem. Soc., Chem. Commun.*, **1991**, 1104; (c) P. Andrews, J. M. Corker, J. Evans, M. Webster, *J. Chem. Soc. Dalton Trans.*, **1994**, 1337; (d) D. Gogg, M. Conyngham, J. M. Corker, A. J. Dent, J. Evans, R. C. Farrow, V. L. Kambhampati, A. F. masters, D. N. MacLeod, C. A. Ramsdale, G. Salvini, *Chem. Commun.*, **1996**, 647.
35. (a) S. G. Fiddy, J. Evans, T. Neisium, M. A. Newton, N. Tsoureas, A. A. D. Tulloch, A. A. Danopoulos, *Chem. Eur. J.*, **2007**, *13*, 3652; see also the related work (b) J. Evans, L. O. Neil, V. L. Kambhampati, G. Rayner, S. Turin, A. Genge, A. J. Dent, T. Neisius, *J. Chem. Soc., Dalton Trans.*, **2002**, 2207.
36. M. Tromp, G. P. F. van Strijdonck, S. S. van Berkel, A. van den Hoogenband, M. C. Feiters, B. de Bruin, S. G. Fiddy, A. M. J. van Eerden, J. A. van Bokhoven, P. W. N. M. van Leeuwen, D. C. Koningsberger, *Organometallics*, **2010**, *29*, 3085.
37. (a) J. O. Moulin, J. Evans, D. S. McGuinness, G. Reid, A. J. Rucklidge, R. P. Tooze, M. Tromp, *Dalton Trans.*, *2008*, 1177; the XAS-based catalysis investigation of paramagnetic heavy congener of Mo^{III}, see (b) S. A. Bartlett, P. P. Wells, M. Nachtegaal, A. J. Dent, G. Cibin, G. Reid, J. Evans, M. Tromp, *J. Catalysis*, **2011**, *284*, 247.
38. M. P. Feth, C. Bolm, J. P. Hildebrand, M. Köhler, O. Beckmann, M. Bauer, R. Ramamonjisoa, H. Bertagnolli, *Chem. Eur. J.*, **2003**, *9*, 1348.
39. S. Diazo-Moreno, D. T. Bowron, J. Evans, *Dalton Trans.*, **2005**, 3814.
40. H. Asakura, T. Shishido, T. Tanaka, *J. Phys. Chem. A.*, **2012**, *116*, 4029.
41. C. He, G. Zhang, J. Ke, H. Zhang, J. T. Miller, A. J. Kropf, A. Lei, *J. Am. Chem. Soc.* **2013**, *135*, 488.
42. R. K. Hocking, E. I. Solomon, *Molecular Electronic Structures of Transition Metal Complex I, Structure and Bonding 142*, ed. by D. M. P. Mingos, P. Day, J. P. Dahl, Springer-

Verlag, Berlin, 2012; pp. 155–184.

43. M. Bauer C. Gastl, *Phys. Chem. Chem. Phys.*, **2010**, *12*, 5575.
44. A. Welther, M. Bauer, M. Mayer, A. J. von Wangelin, *ChemCatChem*, **2012**, *4*, 1088.
45. R. Schoch, W. Desens, T. Werner, M. Bauer, *Chem. Eur. J.*, **2013**, *19*, 15816.
46. S. L. Daifuku, M. H. Al-Afyouni, B. E. R. Snyder, J. L. Kneebone, M. L. A. Neidig, *J. Am. Chem. Soc.*, **2014**, *36*, 9132.
47. T. Hatakeyama, Y. Fujiwara, Y. Okada, T. Itoh, T. Hashimoto, S. Kawamura, K. Ogata, H. Takaya, M. Nakamura, *Chem. Lett.*, **2011**, *40*, 1030.
48. S. Kawamura, M. Nakamura, *Chem. Lett.*, **2013**, *42*, 183.
49. D. Noda, Y. Sunada, T. Hatakeyama, M. Nakamura, H. Nagashima, *J. Am. Chem. Soc.*, **2009**, *131*, 6078.
50. R. B. Bedford, P. B. Brenner, E. Carter, P. M. Cogswell, M. F. Haddow, J. N. Harvey, D. M. Murphy, J. Nunn, C. H. Woodall, *Angew. Chem. Int. Ed.*, **2014**, *53*, 1804.
51. Von W. Seidel, K.-J. Lattermann, *Z. Anorg. Allg. Chem.*, **1982**, *488*, 69.
52. C.-L. Sun, H. Krause, A. Fürstner, *Adv. Synthe. Catal.*, **2014**, *356*, 1281.
53. For multi-gram scale synthesis of $FeMes_2$(SciOPP) **3**, $FeCl_2$ salt was used as a highly cost-effective iron source, although both $FeCl_2$ and $FeBr_2$ gave **3** via this procedure.
54. E. J. Hawrelak, W. H. Bernskoetter, E. Lobkovsky, G. T. Yee, E. Bill, P. J. Chirik, *Inorg. Chem.*, **2005**, *44*, 3103.
55. J. Chatt, B. L. Shaw, *J. Chem. Soc.*, **1961**, 285.
56. J. P. Collman, J. L. Hoard, N. Kim, G. Lang, C. A. Reed, *J. Am. Chem. Soc.*, **1975**, *97*, 2676.
57. (a) C. G. Barraclough, R. L. Martin, S. Mitra, R. C. Sherwood, *J. Chem. Phys.*, **1970**, *53*, 1643; (b) S. Y. Ha, J. Park, T. Ohta, G. Kwag, S. Kim, *Electrochem. Solid-State Lett.*, **1999**, *2*, 461.
58. A. R. Hermes, G. S. Girolami, *Organometallics*, **1987**, *6*, 763.
59. The Fe K-edge (7.11 KeV) XAS data were corrected by transmission mode and calibrated

by using an iron metal foil as a reference sample. For solution phase XAS, air- and moisture-sensitive sample solutions were transferred into a specially designed quarts-made solution cell with Teflon-made windows in the argon-filled glovebox.

60. T. E. Westre, P. Kennepohl, J. G. DeWitt, B. Hedman, K. O. Hodgson, E. I. Solomon, *J. Am. Chem. Soc.*, **1997**, *119*, 6297.
61. T. Yamamoto, *X-Ray Spectrum*, **2008**, *37*, 572.
62. The fitting calculation was performed by FEFF9 program (revision 9.6.4) embedded with Artemis where the theoretical scattering paths were generated from crystallographic coordinate based on the single crystal X-ray structures of **2** and **3** depicted in Figs. 1(a) and 1(b). See, SI Figs. S22 and S23, and Tables S2 and S3. For FEFF9 program, see also; J. J. Rehr, J. J. Kas, F. D. Vila, M. P. Prange, K. Jorissen, *Phys. Chem. Chem. Phys.* **2010,** *12*, 5503.
63. See SI Figs. S14 and S15 for the comparison with the XANES and EXAFS spectra of **1** with 2.0 equiv. of MesMgBr and authentic **3** in THF solution.60.